BASIC RESEARCH www.jasn.org

Human Induced Pluripotent Stem Cell–Derived Podocytes Mature into Vascularized Glomeruli upon Experimental Transplantation

Sazia Sharmin,* Atsuhiro Taguchi,* Yusuke Kaku,* Yasuhiro Yoshimura,*† Tomoko Ohmori,* Tetsushi Sakuma,‡ Masashi Mukoyama,† Takashi Yamamoto,‡ Hidetake Kurihara,§ and Ryuichi Nishinakamura*‖

*Department of Kidney Development, Institute of Molecular Embryology and Genetics, and †Department of Nephrology, Faculty of Life Sciences, Kumamoto University, Kumamoto, Japan; ‡Department of Mathematical and Life Sciences, Graduate School of Science, Hiroshima University, Hiroshima, Japan; §Division of Anatomy, Juntendo University School of Medicine, Tokyo, Japan; and ‖Japan Science and Technology Agency, CREST, Kumamoto, Japan

ABSTRACT

Glomerular podocytes express proteins, such as nephrin, that constitute the slit diaphragm, thereby contributing to the filtration process in the kidney. Glomerular development has been analyzed mainly in mice, whereas analysis of human kidney development has been minimal because of limited access to embryonic kidneys. We previously reported the induction of three-dimensional primordial glomeruli from human induced pluripotent stem (iPS) cells. Here, using transcription activator–like effector nuclease-mediated homologous recombination, we generated human iPS cell lines that express green fluorescent protein (GFP) in the *NPHS1* locus, which encodes nephrin, and we show that GFP expression facilitated accurate visualization of nephrin-positive podocyte formation *in vitro*. These induced human podocytes exhibited apicobasal polarity, with nephrin proteins accumulated close to the basal domain, and possessed primary processes that were connected with slit diaphragm–like structures. Microarray analysis of sorted iPS cell–derived podocytes identified well conserved marker gene expression previously shown in mouse and human podocytes *in vivo*. Furthermore, we developed a novel transplantation method using spacers that release the tension of host kidney capsules, thereby allowing the effective formation of glomeruli from human iPS cell–derived nephron progenitors. The human glomeruli were vascularized with the host mouse endothelial cells, and iPS cell–derived podocytes with numerous cell processes accumulated around the fenestrated endothelial cells. Therefore, the podocytes generated from iPS cells retain the podocyte-specific molecular and structural features, which will be useful for dissecting human glomerular development and diseases.

J Am Soc Nephrol 27: 1778–1791, 2016. doi: 10.1681/ASN.2015010096

The glomerulus is the filtering apparatus of the kidney and contains three types of cells: podocytes, vascular endothelial cells, and mesangial cells. Podocytes cover the basal domains of the endothelial cells *via* the basement membrane and play a major role in the filtration process.[1,2] Podocytes possess multiple cytoplasmic protrusions. The primary processes are complicated by the further stemming of smaller protrusions (secondary processes or foot processes), which interdigitate with those from neighboring podocytes. The gaps between these foot processes are connected with the slit diaphragm, which is detectable only by electron microscopy. The molecular nature of the slit diaphragm was initially revealed by identification of *NPHS1* as the gene responsible for Finnish-type

Received January 26, 2015. Accepted August 26, 2015.

S.S. and A.T. contributed equally to this work.

Published online ahead of print. Publication date available at www.jasn.org.

Correspondence: Dr. Ryuichi Nishinakamura, Department of Kidney Development, Institute of Molecular Embryology and Genetics, Kumamoto University, 2-2-1 Honjo, Chuo-ku, Kumamoto 860-0811, Japan. Email: ryuichi@kumamoto-u.ac.jp

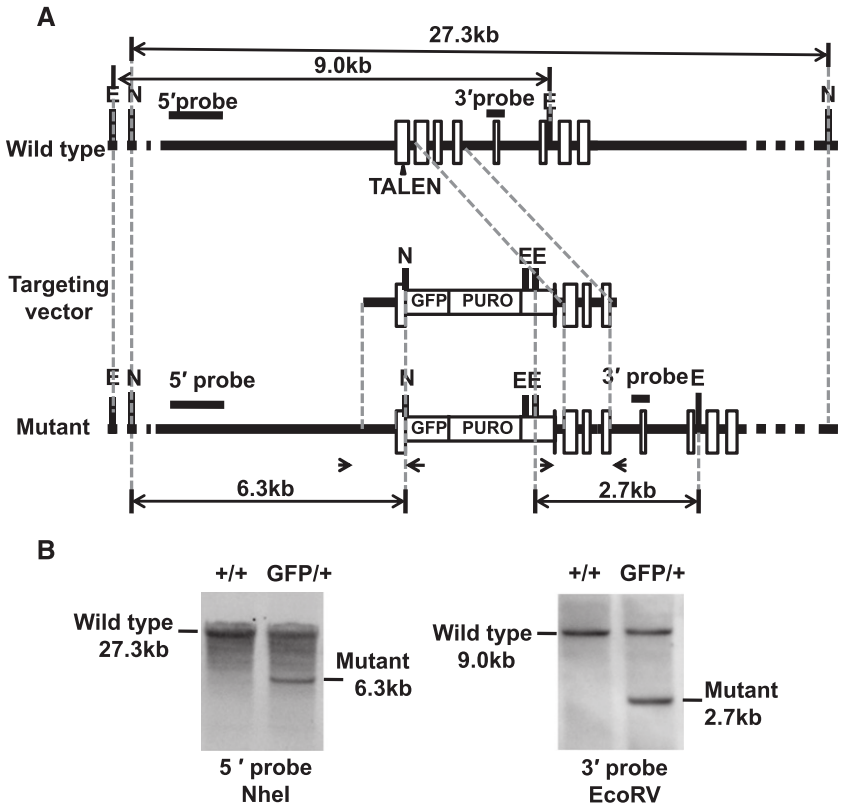

Figure 1. Successful generation of *NPHS1-GFP* iPS cells by homologous recombination. (A) Strategy for targeting the human *NPHS1* locus. The *GFP* cassette was inserted upstream of the *NPHS1* start codon. The puromycin-resistance cassette (PURO) is flanked by loxP sites. Positions for primers and probes for screening are indicated. E, *EcoRV*; N, *Nhe*I. (B) Southern blot of control (+/+) and *NPHS1-GFP* (GFP/+) clones. Genomic DNA was digested and hybridized with the indicated probes.

congenital nephrotic syndrome.[3] The nephrin protein encoded by *NPHS1* intercalates with those from neighboring cells, thus forming a molecular mesh that hinders serum proteins of high molecular weight from leaking into the urine.[4,5] To date, many slit diaphragm–associated proteins have been identified, including *NPHS2* (encoding podocin) and *NEPH1*, mutations that cause proteinuria in humans and/or mice.[6,7]

Podocytes are derived from nephron progenitors that reside in the embryonic kidney and express transcription factor Six2.[8] Upon Wnt stimulation, the nephron progenitors undergo mesenchymal-to-epithelial transition and form a tubule.[9] This tubule changes its shape; one end forms the glomerulus with podocytes inside, which is surrounded by a Bowman's capsule. Meanwhile, vascular endothelial cells and mesangial cells migrate into the developing glomeruli, thus connecting the glomeruli with circulation.[2] In these processes, several transcription factors, including Wt1, regulate expression of nephrin in podocytes.[10] Apical junctions are initially formed between the presumptive podocytes, but the apical domain loses its direct contact with that of the neighboring cells, thus forming the characteristic podocyte shape. Nephrin is eventually localized to the site close to the basal domain and contributes to the formation of the slit diaphragm.[2] The molecular mechanisms underlying podocyte development have been extensively studied in mice. However, because of limited access to human embryos, relatively little is known regarding transcription profiles of podocytes and glomerulogenesis in humans.[4,11,12]

We have recently induced the nephron progenitors from mouse embryonic stem (ES) cells and human induced pluripotent stem (iPS) cells by redefining the *in vivo* origin of the nephron progenitors.[13] The induced progenitor aggregates readily form three-dimensional primordial glomeruli and renal tubules upon Wnt stimulation *in vitro*. To analyze the detailed structures and transcription profiles of the induced podocytes, we have here inserted the *GFP* gene into the *NPHS1* locus of human iPS cells *via* homologous recombination using transcription activator–like effector nucleases (TALENs)[14] and generated glomeruli with green fluorescent protein (GFP)-tagged podocytes.

RESULTS

Fluorescent Visualization of Human Glomerular Podocytes Generated from *NPHS1-GFP* iPS Cells

To visualize developing human podocytes *in vitro*, we inserted a gene encoding GFP into the *NPHS1* locus of human iPS cells by homologous recombination (Figure 1A). We first constructed a pair of plasmids expressing TALENs targeted in close proximity to the *NPHS1* start codon. When tested in HEK 293 cells, these plasmids efficiently deleted the *NPHS1* gene (Supplemental Figure 1A). We then introduced these TALEN plasmids, along with a targeting vector containing the *GFP* gene and the homology arms, into human iPS cells. This resulted in efficient homologous recombination and isolation of heterozygous *GFP* knock-in (*NPHS1-GFP*) clones (Figure 1B, Supplemental Figure 1, B and C).

We differentiated these *NPHS1-GFP* iPS clones toward the nephron progenitors and subsequently combined them with murine embryonic spinal cord, which is a potent inducer of tubulogenesis, as we previously reported.[13] Four days after recombination, spotty GFP signals could be observed, and the number and intensity of GFP signals increased thereafter until day 9 (Figure 2A, Supplemental Figure 2A). We observed GFP signals in all the examined samples from seven independent experiments (a total of 50 samples). Some of the signals started in a crescent shape and gradually changed into round structures (Figure 2A, lower panels), which suggests that

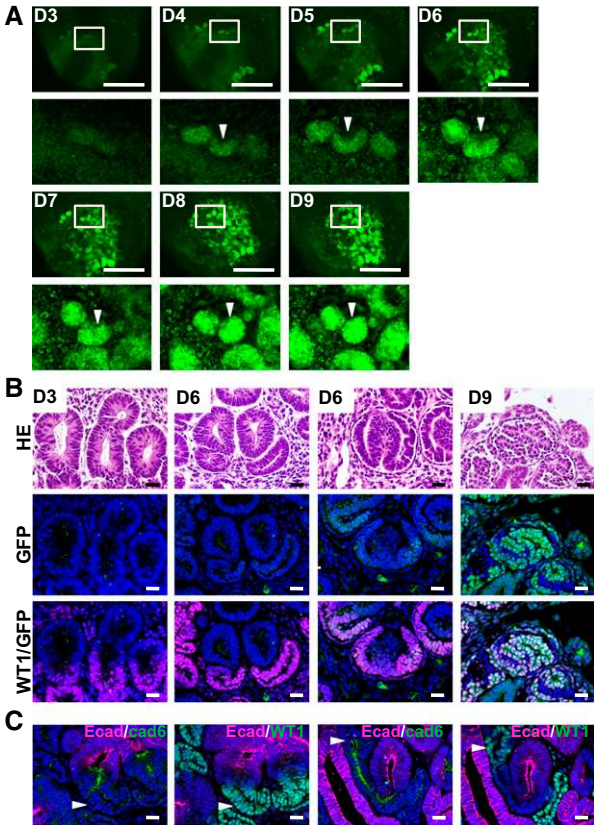

Figure 2. Fluorescent visualization of human glomerular podocytes generated from *NPHS1-GFP* iPS cells. (A) Morphologic changes of GFP-positive glomeruli during differentiation *in vitro*. The nephron progenitors induced from *NPHS1-GFP* iPS cells were combined with murine embryonic spinal cord and cultured for the indicated time. Lower panels: higher magnification of the areas marked by rectangles in the upper panels. Note the shape changes of the glomerulus (arrowheads). Scale bars: 500 μm. (B) Histologic sections of glomeruli developing *in vitro*. Tissues at day 3, 6, and 9 after recombination with the spinal cord were analyzed. Top panels: Hematoxylin-eosin (HE) staining. Middle panels: GFP (green) staining. Bottom panels: dual staining with GFP and WT1. Nuclei were stained with 4′,6-diamidino-2-phenylindole (DAPI: blue). Scale bars: 20 μm. (C) Presumptive S-shaped bodies observed at day 4 (left two panels) and day 6 (right two panels). Serial sections were stained with E-cadherin (Ecad: magenta)/cadherin-6 (cad6: green) and E-cadherin (magenta)/WT1 (green). Arrowheads: WT1-positive presumptive glomerular regions. Scale bars: 20 μm.

human glomerular formation *in vitro* may be visualized. Therefore, we examined glomerulogenesis using sections of the explants. At day 3, only tubular structures were observed and GFP-positive cells were undetectable (Figure 2B). At day 4, structures that resembled S-shaped bodies were observed, in which proximo-distal specification occurred toward the presumptive distal (E-cadherin+) and proximal (cadherin-6+) renal tubules and glomerular podocytes (WT1+) (Figure 2C). At day 6, various forms of primordial glomeruli were observed, and most of the GFP signals overlapped with those of WT1 (Figure 2B). We ordered these glomeruli according to GFP intensity, which is likely to reflect the chronologic order of development. Weakly GFP-positive (and WT1-positive) limbs appeared at one end of the tubules, which elongated to surround the renal tubules. GFP intensity increased when the podocyte layers were convoluted. At day 9, strongly GFP-positive round glomeruli were formed. These histologic changes are consistent with the previous observations of human glomeruli in aborted fetuses.[15] Thus, we succeeded in visualizing human podocyte development and glomerulogenesis *in vitro*. Interestingly, some, but not all, of the Bowman's capsule cells were positive for GFP and nephrin (Supplemental Figure 2B), suggesting that these cells are not completely specified yet. Indeed, transient nephrin expression in some capsule cells was reported *in vivo*.[16]

Induced Podocytes Exhibit Apicobasal Polarity and Basally Localized Nephrin

We analyzed day 9 sections at higher resolution to examine the apicobasal polarity of the induced podocytes. GFP was detected in the nuclei and cytoplasm of most cells in the round glomeruli (Figure 3A) because we did not attach any localization signal to GFP when generating *NPHS1-GFP* iPS cells. Nephrin proteins were distributed in a linear fashion in the iPS cell–derived glomeruli and at one end of the WT1-positive podocyte layer

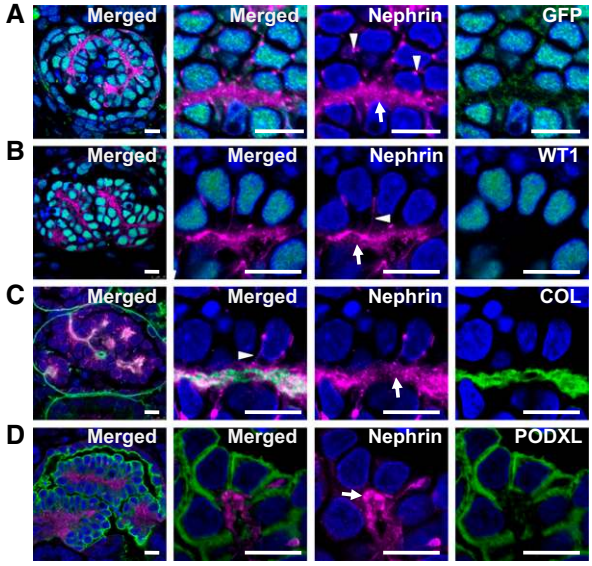

Figure 3. Induced podocytes exhibit apicobasal polarity and basally localized nephrin. (A) Nephrin (magenta) and GFP (green) staining of the induced glomerulus at day 9. (B) Nephrin (magenta) and WT1 (green) staining. (C) Nephrin (magenta) and type IV collagen (COL: green) staining. (D) Nephrin (magenta) and podocalyxin (PODXL: green) staining. The left columns are at lower magnification to show a whole glomerulus. The right two columns are singly stained, while the left two columns represent merged images. Arrows: nephrin proteins localized to the basal domain; arrowheads: nephrin-positive dot-like or filamentous structures. Scale bars: 10 μm.

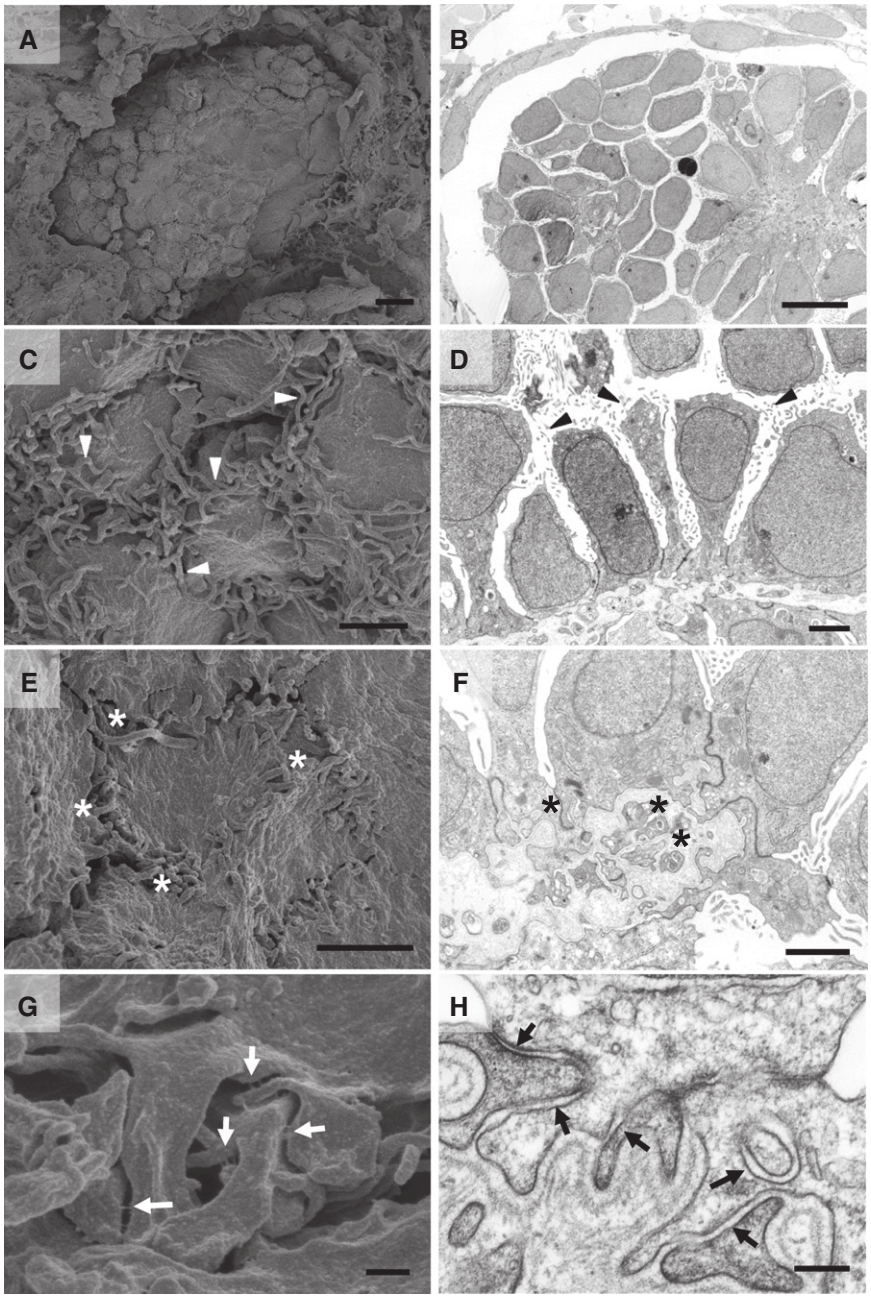

Figure 4. Induced podocytes possess primary processes with the immature slit diaphragm–like structures. (A and B) Induced glomerulus covered with a Bowman's capsule shown by (A) scanning and (B) transmission electron microscopy. (C) Induced podocytes observed by scanning electron microscopy. Multiple microvilli are observed on the apical surface (arrowheads). (D) Aligned podocytes, which attach to each other at sites close to the basal region, shown by transmission electron microscopy. Multiple microvilli are observed on the apical surface (arrowheads). (E) Primary processes shown by scanning electron microscopy (asterisks). Podocytes from the basal side are shown. (F) Primary processes shown by transmission electron microscopy (asterisks). (G) Slit diaphragm–like structures between the primary processes (arrows), shown by scanning electron microscopy. (H) Primary processes with slit diaphragm–like structures (arrows), shown by transmission electron microscopy. Scale bars: A and B: 10 μm; C–F: 2 μm; G and H: 0.2 μm.

(Figure 3, A and B). These expression patterns significantly overlapped with those of type IV collagen, which was accumulated on the basal side of the podocytes (Figure 3C). In contrast, podocalyxin, an apical marker, was expressed in a manner mutually exclusive of nephrin (Figure 3D). Therefore, the induced podocytes exhibited a well established apicobasal polarity and nephrin proteins were properly localized at the basal side, where the presumptive slit diaphragm should be formed. We also observed nephrin-positive dots on the lateral side of the podocytes (Figure 3A, arrowheads), as reported in human developing podocytes *in vivo*.[15] We found that these dots actually represent the filamentous structures encompassing the basal to the lateral side of the podocytes (Figure 3, B and C, arrowheads). Although further investigation is required, this may reflect the transit state of nephrin proteins shifting from the apical to the basal domain of the induced podocytes.

Induced Podocytes Possess Primary Processes with the Slit Diaphragm–Like Structures

We further analyzed the morphology of the induced glomeruli by electron microscopy. Both scanning and transmission electron microscopy showed well organized glomeruli surrounded by Bowman's capsules (Figure 4, A and B). Interestingly, numerous microvilli were detected in the apical domain of the induced podocytes (Figure 4, C and D). Similar microvilli were reported in developing *in vivo* podocytes in humans.[17,18] The podocytes were attached to each other at sites close to the basal region (Figure 4D). Inspection of the basal side of the induced podocytes by scanning microscopy identified multiple protrusions (Figure 4E), which were confirmed by transmission microscopy (Figure 4F). Higher magnification clearly showed bridging structures between the protrusions, which may represent an immature form of the slit diaphragm (Figure 4, G and H, Supplemental Figure 3, A–C). Thus, this is the first *in vitro* generation of mammalian podocytes with slit diaphragm–like structures from pluripotent stem cells. However, because typical interdigitation of the protrusions is lacking,

they are likely to represent primary processes but not secondary processes (foot processes).

Induction of Podocytes from Human *NPHS1-GFP* iPS Cells Enables Their Efficient Isolation

We next tried to purify the GFP-positive podocytes at day 9 by FACS. Of the induced cells, 7.45%±0.72% (mean±SEM from five independent induction experiments) were positive for GFP (Figure 5A, left panel). We also found that the monoclonal antibody against the extracellular domain of nephrin (48E11),[19] in combination with the anti-podocalyxin antibody, was useful for sorting developing podocytes. Of the GFP-positive cells, 94.0% were positive for both nephrin and podocalyxin (Figure 5A, middle panel), while most of the GFP-negative cells (97.5%) were negative for both markers (Figure 5A, right panel). Thus, GFP faithfully mimics nephrin expression and podocytes were enriched in the GFP-positive population. Quantitative RT-PCR analysis of sorted cells confirmed the differential expression of several podocyte markers, such as *NPHS2* (encoding podocin) and *synaptopodin* (Figure 5B). When the sorted GFP-positive cells were cultured for 3 days, the cells expressed WT1 in nuclei and podocalyxin on the cell surface (Figure 5C). Nephrin and GFP were detected on the cell surface membrane and in the cytoplasm, respectively, at day 7 of culture, although expression levels were lower than before the start of the culture. These results indicate that induction from *NPHS1-GFP* iPS cells enables efficient isolation of developing human podocytes.

GFP-Positive–Induced Podocytes Show Transcriptional Profiles That Overlap with Those of Mouse and Human Podocytes *In Vivo*

To obtain comprehensive transcription profiles of the iPS cell–derived podocytes, we performed microarray analysis at day 9. We detected 2985 probes that were enriched in GFP-positive podocytes compared with GFP-negative cells. Of these, the top 300 genes were used for unbiased cluster analysis against microarray data from a wide variety of human tissues (Supplemental Figure 4, A and C).[20] Genes enriched in the GFP-positive podocytes had variable tissue specificity. For example, *NPHS2* was selectively expressed in the kidney or fetal kidney tissues. However, *synaptopodin* and *FOXC2* were sorted into the ubiquitously expressing cluster. *Dendrin* was assigned to a cluster enriched in the neuronal tissues. These results suggest a single molecule is not sufficient to confirm the identity of podocytes. Therefore, we compared our gene list of GFP-positive human podocytes with the published microarray analyses of adult human glomeruli and adult podocytes from *Mafb-GFP* transgenic mice.[11,21] Overall, 190 probes were overlapping among the three gene sets (Figure 5D, Supplemental Table 1, Table 1). These included typical slit diaphragm–related genes, such as *NPHS1*, *NPHS2*, *CD2AP*,[22] chloride intracellular channel protein 5 (*CLIC5*),[23] and *dendrin*,[24,25] and basolateral adhesion molecules such as claudin 5 and integrin $\alpha 3$.[26,27] *Phospholipase $\varepsilon 1$* and nonmuscle myosin heavy chain 9 (*Myh9*), causative genes for hereditary kidney diseases,[28–30] were also included. Transcription factors that have important roles in podocyte development, including *WT1*, *MAFB*, *FOXD1*, and *TCF21*, as well as vascular attractants such as *VEGFA* and *semaphorin*, were also expressed.[1,2,31] Interestingly, when these selected overlapping genes were used for the cluster analysis against the microarray data from various organs described above, kidney and fetal kidney were segregated as separate clusters, suggesting the kidney-biased features of the overlapping gene set (Supplemental Figure 4B).

We also identified genes common to GFP-positive podocytes and adult human glomeruli (Figure 5D, Supplemental Table 2), and genes common to GFP-positive podocytes and mouse adult podocytes (Figure 5D, Supplemental Table 3). The former includes *BMP7*,[32] while the latter includes *NEPH1 (KIRREL)*, *FOXC2*, *ROBO2*, and *EPHRIN-B1*.[7,33–36] These results indicated that the typical transcriptional profiles are well conserved among our podocytes generated *in vitro* as well as mouse and human podocytes *in vivo*. In addition, extracellular matrix components characteristic of glomeruli at the capillary loop stage, *laminin$\alpha 5/\beta 2/\gamma 1$* isoforms (corresponding to laminin 521) and type IV collagen $\alpha 4/\alpha 5$,[37] were detected, the latter of which is the causative gene for Alport syndrome. These data indicate that the transition to these mature forms from immature laminin 111 and collagen $\alpha 1/\alpha 2$ has already occurred *in vitro*.

Taken together, our podocytes induced *in vitro* possessed the typical features of those *in vivo*, not only in morphology but also in transcription profiles, further supporting the authenticity of our human iPS cell induction protocol. In addition, genes exclusively expressed in the GFP-positive podocytes are worthy of further investigation because they may include genes specific to developing human podocytes, a possibility that has not been addressed to date (Figure 5D, Supplemental Table 4).

Transplanted iPS Cell–Derived Nephron Progenitors Form Vascularized Glomeruli

We next examined whether glomeruli generated from iPS cells integrated with the vascular endothelial cells. The iPS cell–derived nephron progenitor spheres were induced by spinal cord for 1 day *in vitro* to initiate tubulogenesis and were then transplanted beneath the kidney capsule of immunodeficient mice. We also cotransplanted mixed aggregates of human umbilical vein endothelial cells (HUVECs) and mesenchymal stem cells (MSCs) because these cells are useful for the generation of vascularized organ buds *in vitro*.[38,39] When these aggregates were transplanted using a conventional method that we used for the transplantation of mouse ES cell–derived nephron progenitors,[13] minimal nephron differentiation was observed at 10 days after transplantation (n=4) (Figure 6A). Because human iPS cell–derived aggregates were larger (approximately 1000 μm in diameter) than those from mouse ES cells (approximately 600 μm) and were instantly flattened upon transplantation (Supplemental Figure 5A), we hypothesized that

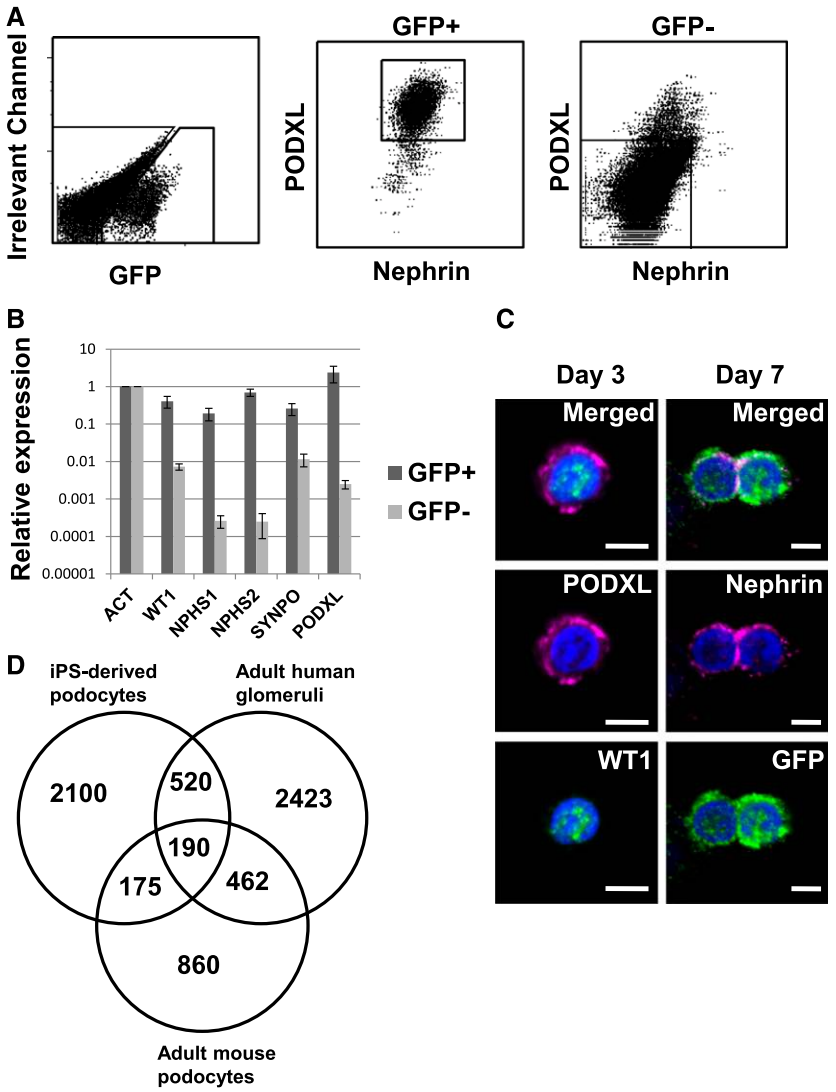

Figure 5. Induction of podocytes from human *NPHS1-GFP* iPS cells enables their efficient isolation. (A) FACS analysis of induced tissues at day 9. Almost 8% of cells are positive for GFP in this representative experiment (left panel). Nephrin and podocalyxin (PODXL) expression in the GFP-positive or -negative fraction (middle and right panel, respectively). (B) Quantitative RT-PCR analysis of GFP-positive and -negative fractions. Average and SEM from three independent experiments are shown. β-ACT, β-actin; SYNPO, synaptopodin. (C) Immunostaining of podocytes cultured for the indicated times after sorting GFP-positive cells. Scale bars: 5 μm. (D) Venn diagram of the transcription profiles of podocytes. Microarray data of GFP-positive podocytes are compared with those of human adult glomeruli and murine podocytes.

mechanical tension of the capsule may have hampered nephron differentiation. Therefore, we inserted two agarose rods of 1100 μm diameter in a V-shaped position to release tension and secure a space for the transplanted aggregates (Figure 6B). We also soaked the rods with VEGF to enhance vasculogenesis.[31] As a result, we observed immature glomerular formation at day 10 in the transplants, accompanied by blood vessels integrating into these glomeruli (n=5) (Figure 6, C and D). The vessels were preferentially clustered in the glomeruli among the grafted tissue (Figure 6D), suggesting that the iPS cell–derived podocytes possess the potential to attract vasculature. This is also consistent with microarray data showing *VEGFA* expression in our induced podocytes.

At day 20 after transplantation, we observed enlarged transplanted tissues beneath the capsule (Supplemental Figure 5B). Histologic examination revealed excessive growth of stromal cells of human origin, which were presumably derived from nonrenal tissues that were coinduced with nephron progenitors from iPS cells (n=4) (Figure 6E, Supplemental Figure 5C). Nonetheless, glomeruli were formed and the blood vessels were well integrated into the glomeruli (Figure 6, F and G). Moreover, 90% (135 of 150) of the glomeruli contained red blood cells (Figure 6H). Indeed, some of the glomeruli showed an enlarged Bowman's space and contained eosin-positive precipitation (Figure 6I), which might imply a small amount of urine production. Interestingly, endothelial cells in the induced glomeruli were of mouse origin (Figure 6G, Supplemental Figure 5D). HUVEC-derived endothelial cells were not integrated into the iPS cell–derived glomeruli but were located separately from the sites of nephron formation (Supplemental Figure 5E). Therefore, HUVEC may not be competent to interact with human podocytes.

The anti-human specific podocalyxin antibody stained the apical domains of the iPS cell–derived podocytes, but not those of the host mouse podocytes (Supplemental Figure 5F). Nephrin protein in induced podocytes was localized at the basal side that faced the vascular endothelial cells (Figure 6J), suggesting the emergence of filtering apparatus. Electron microscopic analyses of two additional samples at day 20 showed that iPS cell–derived podocytes accumulated around, and were closely associated with, endothelial cells (Figure 7A). The induced podocytes developed numerous complex cell processes, as well as a linear basement membrane, at interfaces with endothelial cells (Figure 7B). The distances between the cell processes of some podocytes were enlarged, and slit diaphragm–like structures were formed between the processes located above the basement membrane (Figure 7C). Each of these diaphragms appeared as an electron-dense line (approximately 35 nm wide, 10 nm thick) bridging adjacent

Table 1. Genes common to iPS cell–derived podocytes *in vitro*, human glomeruli, and mouse podocytes *in vivo*

Gene Symbol	Gene Name	iPS Cell–Derived Podocytes	Human Glomeruli	Mouse Podocytes
CLIC5	Chloride intracellular channel 5	141.94	6.48	9.10
NPHS1	Nephrosis 1, congenital, Finnish type (nephrin)	141.30	10.41	22.75
CLIC5	Chloride intracellular channel 5	107.11	6.48	9.10
NPHS2	Nephrosis 2, idiopathic, steroid-resistant (podocin)	99.93	9.99	19.95
PODXL	Podocalyxin-like	78.48	9.34	26.60
PTPRO	Protein tyrosine phosphatase, receptor type, O	62.91	24.68	26.69
CLDN5	Claudin 5	61.39	14.33	5.39
ITGA3	Integrin, α3 (antigen CD49C, α3 subunit of VLA-3 receptor)	51.41	9.33	9.98
CTGF	Connective tissue growth factor	38.19	8.31	4.48
NPR1	Natriuretic peptide receptor 1	33.39	4.83	7.31
TGFBR3	Transforming growth factor, β receptor III	32.29	2.06	2.82
FOXD1	Forkhead box D1	27.96	3.87	18.67
MAFB	v-maf avian musculoaponeurotic fibrosarcoma oncogene homolog B	26.91	14.07	8.56
BCAM	Basal cell adhesion molecule (Lutheran blood group)	22.95	2.04	2.71
RAPGEF3	Rap guanine nucleotide exchange factor (GEF) 3	22.71	5.02	2.04
SEMA3G	Sema domain, Ig domain, short basic domain, secreted, (semaphorin) 3G	21.56	31.46	6.33
WT1	Wilms tumor 1	20.93	14.02	19.15
DDN	Dendrin	19.22	9.91	4.25
HSPB8	Heat shock 22-kDa protein 8	18.38	6.53	4.66
ST3GAL6	ST3 β-galactoside α-2,3-sialyltransferase 6	17.31	9.95	4.91
TCF21	Transcription factor 21	16.82	31.46	14.60
ELF4	E74-like factor 4 (ets domain transcription factor)	15.79	3.60	4.34
MAFB	v-maf avian musculoaponeurotic fibrosarcoma oncogene homologue B	15.26	14.07	8.56
NTNG1	Netrin G1	15.12	2.66	1.89
LAMA5	Laminin, α5	14.59	2.27	2.32
ARHGAP29	Rho GTPase activating protein 29	14.09	2.40	1.98
PLCE1	Phospholipase C, ε1	14.02	29.93	33.24
PLCE1	Phospholipase C, ε1	14.00	29.93	33.24
VAMP5	Vesicle-associated membrane protein 5	13.44	7.08	2.64
ANXA1	Annexin A1	13.32	11.09	10.61
HTRA1	HtrA serine peptidase 1	13.06	11.95	4.24
MPP5	Membrane protein, palmitoylated 5 (MAGUK p55 subfamily member 5)	12.96	2.90	3.20
VEGFA	Vascular endothelial growth factor A	12.93	2.33	6.20
VEGFA	Vascular endothelial growth factor A	12.80	2.33	6.20
CORO2B	Coronin, actin binding protein, 2B	11.74	7.54	4.86
MXRA8	Matrix-remodelling associated 8	11.08	6.58	2.98
HSPA12A	Heat shock 70-kDa protein 12A	10.65	3.66	4.43
SYNPO	Synaptopodin	9.66	19.26	7.40
PDLIM5	PDZ and LIM domain 5	9.32	2.87	2.30
NTNG1	Netrin G1	8.98	2.66	1.89
MAGI2	Membrane associated guanylate kinase, WW and PDZ domain containing 2	8.25	25.02	16.28
LEPREL1	Leprecan-like 1	7.46	3.79	3.14
RAPGEF3	Rap guanine nucleotide exchange factor (GEF) 3	7.31	5.02	2.04
DAG1	Dystroglycan 1 (dystrophin-associated glycoprotein 1)	6.89	5.78	4.12
FOXC1	Forkhead box C1	6.45	6.92	2.71
SPARC	Secreted protein, acidic, cysteine-rich (osteonectin)	6.28	9.20	8.65
PDPN	Podoplanin	6.28	8.99	17.51
TJP1	Tight junction protein 1	6.20	4.15	8.42
TM4SF1	Transmembrane 4 L six family member 1	6.06	3.66	5.99
AMIGO2	Adhesion molecule with Ig-like domain 2	6.02	17.63	3.22
TRAM2	Translocation associated membrane protein 2	5.74	11.62	2.20
LEPROT	Leptin receptor overlapping transcript	5.72	2.76	1.96
FAM65A	Family with sequence similarity 65, member A	5.47	6.51	13.42
PLOD2	Procollagen-lysine, 2-oxoglutarate 5-dioxygenase 2	5.33	5.50	5.84
MYO1E	Myosin IE	5.25	6.36	9.88

Table 1. Continued

Gene Symbol	Gene Name	iPS Cell–Derived Podocytes	Human Glomeruli	Mouse Podocytes
PDLIM5	PDZ and LIM domain 5	5.18	2.87	2.30
TM4SF1	Transmembrane 4 L six family member 1	4.86	3.66	5.99
MYH9	Myosin, heavy chain 9, nonmuscle	4.67	4.38	4.07
MGAT5	Mannosyl (α-1,6-)-glycoprotein β-1,6-N-acetyl-glucosaminyltransferase	4.65	14.53	11.89
THSD7A	Thrombospondin, type I, domain containing 7A	4.65	2.58	13.87
SYNPO	Synaptopodin	4.62	19.26	7.40
LAMB2	Laminin, β2 (laminin S)	4.53	5.00	3.54
LAMB2	Laminin, β2 (laminin S)	4.52	5.00	3.54
PDLIM2	PDZ and LIM domain 2 (mystique)	4.39	7.40	1.86
KANK1	KN motif and ankyrin repeat domains 1	4.17	3.44	4.34
EHD4	EH-domain containing 4	4.13	4.54	4.46
INF2	Inverted formin, FH2 and WH2 domain containing	4.01	1.68	1.82
MYOF	Myoferlin	3.93	6.07	6.55
CD151	CD151 molecule (Raph blood group)	3.91	4.13	2.25
FYN	FYN oncogene related to SRC, FGR, and YES	3.88	4.72	7.95
KANK1	KN motif and ankyrin repeat domains 1	3.87	3.44	4.34
TAPBP	TAP binding protein (tapasin)	3.84	2.95	1.90
MYH9	Myosin, heavy chain 9, nonmuscle	3.75	4.38	4.07
ST6GAL1	ST6 β-galactosamide α-2,6-sialyltranferase 1	3.72	1.52	5.98
ITM2C	Integral membrane protein 2C	3.65	1.52	2.11
SPATS2L	Spermatogenesis associated, serine-rich 2-like	3.59	1.86	2.55
F2R	Coagulation factor II (thrombin) receptor	3.54	9.13	3.53
INF2	Inverted formin, FH2 and WH2 domain containing	3.52	1.68	1.82
CPD	Carboxypeptidase D	3.48	2.05	1.86
AHNAK	AHNAK nucleoprotein	3.46	5.70	2.26
SEC14L1	SEC14-like 1 (Saccharomyces *cerevisiae*)	3.36	3.67	1.88
SEC14L1	SEC14-like 1 (*S. cerevisiae*)	3.33	3.67	1.88
ATP8A1	ATPase, aminophospholipid transporter (APLT), class I, type 8A, member 1	3.31	2.13	2.39
NES	Nestin	3.30	14.80	12.04
CD59	CD59 molecule, complement regulatory protein	3.28	2.00	8.21
NLK	Nemo-like kinase	3.23	3.01	4.63
ARAF	v-raf murine sarcoma 3611 viral oncogene homologue	3.21	1.87	2.10
CD2AP	CD2-associated protein	3.20	1.58	3.52
MXRA7	Matrix-remodelling associated 7	3.13	3.78	1.82
NES	Nestin	3.13	14.80	12.04
IL13RA1	Interleukin 13 receptor, α1	3.11	3.60	1.64
TAGLN2	Transgelin 2	3.07	2.49	1.70
NEDD9	Neural precursor cell expressed, developmentally downregulated 9	3.07	3.71	2.65
VAMP2	Vesicle-associated membrane protein 2 (synaptobrevin 2)	3.06	1.79	5.21
HEXIM1	Hexamethylene bis-acetamide inducible 1	2.95	1.56	1.78
TAPBP	TAP binding protein (tapasin)	2.94	2.95	1.90
LAMC1	Laminin, γ1 (formerly LAMB2)	2.93	2.69	2.29
MXRA7	Matrix-remodelling associated 7	2.92	3.78	1.82
CTNNAL1	Catenin (cadherin-associated protein), α-like 1	2.91	2.13	5.97
MYO1D	Myosin ID	2.91	12.33	9.98
TRIB2	Tribbles pseudokinase 2	2.90	7.43	3.31
PTPN21	Protein tyrosine phosphatase, nonreceptor type 21	2.89	1.70	2.12
IL13RA1	Interleukin 13 receptor, α1	2.89	3.60	1.64
MXRA7	Matrix-remodeling associated 7	2.87	3.78	1.82
SPTAN1	Spectrin, α, nonerythrocytic 1	2.86	8.98	1.89
SGMS1	Sphingomyelin synthase 1	2.77	2.28	2.04
APLP2	Amyloid β(A4) precursor-like protein 2	2.72	1.69	2.06
SPTAN1	Spectrin, α, nonerythrocytic 1	2.71	8.98	1.89
MXRA7	Matrix-remodeling associated 7	2.71	3.78	1.82

Table 1. Continued

Gene Symbol	Gene Name	iPS Cell–Derived Podocytes	Human Glomeruli	Mouse Podocytes
PTGER4	Prostaglandin E receptor 4 (subtype EP4)	2.68	22.84	4.09
KDM4C	Lysine (K)-specific demethylase 4C	2.66	1.81	1.87
LEPROT	Leptin receptor overlapping transcript	2.64	2.76	1.96
SIRPA	Signal-regulatory protein α	2.64	8.40	3.15
CTNNAL1	Catenin (cadherin-associated protein), α-like 1	2.62	2.13	5.97
LRRC1	Leucine rich repeat containing 1	2.61	2.58	3.07
IGFBP7	Insulin-like growth factor binding protein 7	2.59	1.51	1.68
CYP1B1	Cytochrome P450, family 1, subfamily B, polypeptide 1	2.58	4.53	2.56
SEL1L	Sel-1 suppressor of lin-12–like (*Caenorhabditis elegans*)	2.58	1.98	1.86
GRK5	G protein–coupled receptor kinase 5	2.58	17.01	4.68
SERINC3	Serine incorporator 3	2.57	2.85	1.52
SEL1L	Sel-1 suppressor of lin-12–like (*C. elegans*)	2.55	1.98	1.86
SERINC3	Serine incorporator 3	2.53	2.85	1.52
C1orf21	Chromosome 1 open reading frame 21	2.51	5.03	4.99

Genes are aligned in the order of fold induction in the GFP-positive versus -negative population of podocytes induced from *NPHS1-GFP* iPS cells (fold induction >2.5). Data on human glomeruli and mouse podocytes are from Ref. 11 and 21, respectively.

cell processes of the iPS cell–derived podocytes (Figure 7D). This feature was also observed *in vivo* and differed from the immature ladder-like structure that was seen between adjacent podocytes cultured exclusively *in vitro* without transplantation (Figure 4). Endothelial cells also produced basement membrane, but it was not fused to that of the podocytes in most cases, thus forming double-layered structures (Figure 7E). Interestingly, endothelial cells were fenestrated with residual diaphragm, a characteristic feature of embryonic glomerular endothelial cells (Figure 7F).[40] Furthermore, an electron-dense substance was detected in the Bowman's space (Figure 7C), as in Figure 6I, implying the possible presence of filtration. Taken together, glomeruli generated from human iPS cells were vascularized and had many morphologic features present in glomeruli *in vivo*.

DISCUSSION

We have inserted *GFP* into the *NPHS1* locus of human iPS cells and successfully differentiated them toward three-dimensional glomeruli. The GFP-positive–induced podocytes possessed apicobasal polarity and were equipped with primary processes and slit diaphragm–like structures. Furthermore, sorted podocytes exhibited typical transcription profiles that overlap with those *in vivo*. These findings underscore the authenticity of our induction protocol. *NPHS1* promoter–driven GFP expression is a good indicator of glomerulus formation. Several groups have reported the induction of kidney tissues *in vitro*,[13,41–43] and our iPS cell lines will be useful for assessing the induction efficiency of glomeruli by each protocol. In addition, we successfully sorted human podocytes using a combination of anti-nephrin and anti-podocalyxin antibodies. These reagents will make genetic GFP integration unnecessary for the purification of podocytes from patient-derived iPS cells, and possibly from more complex *in vivo* tissues.

It is surprising that well organized glomeruli are formed without the other two components of glomeruli: mesangial and vascular endothelial cells. These two cell types are not derived from nephron progenitors, as shown by cell lineage analysis in mice,[8,44,45] and indeed we did not detect these lineages in the induced glomeruli (Supplemental Figure 3D). Thus, glomeruli can self-organize their structures solely from the podocytes derived from nephron progenitors, without any inductive signals from mesangial cells or the vasculature. However, further maturation will be required to reproduce hereditary glomerular diseases. We developed a new transplantation technique using agarose rods to secure a space against the tension evoked by kidney capsules. This technical improvement led to the successful generation, for the first time, of vascularized glomeruli derived from human iPS cells. The induced podocytes exhibited complex cell processes with slit diaphragm–like structures, and linear basement membrane that ran along that of the endothelial cells was formed. Furthermore, endothelial cells were fenestrated, which is a characteristic feature of glomerular endothelial cells. Most experiments used agarose rods soaked with VEGF to potentially accelerate vasculogenesis; however, the absence of VEGF in the rods also caused the formation of vascularized glomeruli (Supplemental Figure 5G). Thus, we can at least conclude that the human iPS cell–derived podocytes expressed sufficient attractants, including VEGF, to recruit endothelial cells.

It is noteworthy that the integrated endothelial cells were of mouse origin from the host animals but were not derived from HUVECs, although both vascular sources were initially located in proximity to the iPS cell–derived transplants. Therefore, human podocytes recruited mouse endothelial cells despite

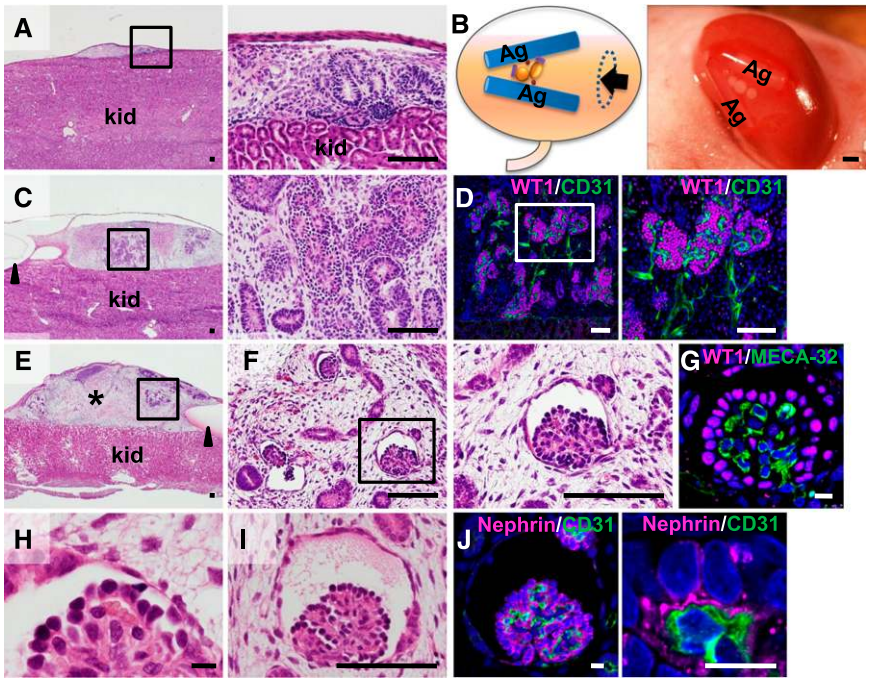

Figure 6. Transplanted iPS cell–derived nephron progenitors form vascularized glomeruli. (A) Hematoxylin-eosin sections of tissues at 10 days after transplantation using a conventional method. Right panel: magnified image of the square in the right panel. kid, kidney of the host mouse. (B) Method for transplantation using solid agarose rods. Right panel: macroscopic view of transplanted tissue under the kidney capsule. Ag, agarose rods. (C) Hematoxylin-eosin sections of the transplanted tissue at day 10 in the presence of the rods. Right panel: magnified images of the square. (D) Vascularized glomeruli at day 10. Staining of WT1 and CD31. Right panel: magnified image of the square in the left panel. (E) Hematoxylin-eosin section of the transplanted tissue at day 20. Middle and right panel: magnified images of the squares in the panels on their left, respectively. *Stromal cells. kid, kidney of the host mouse. (F) Vascularized glomeruli formed upon transplantation at day 20. Left panel: magnified images of panel E. Right panel: magnified image of the square in the left panel. Note the enlarged Bowman's space. (G) The endothelial cells are of mouse origin. Staining of WT1 (magenta) and MECA-32, a marker for mouse-specific endothelial cells (green). (H) Hematoxylin-eosin staining showing red blood cells in the induced glomeruli. (I) Hematoxylin-eosin staining showing the eosin-positive precipitates in the Bowman's space. (J) Staining of nephrin (magenta) and CD31 (green). Right panel shows the basal localization of nephrin. Scale bars: A, C–F, I: 100 μm; B: 1 mm; G, H, J: 10 μm.

species differences, while HUVECs may not be competent to interact with human podocytes. Even when we performed transplantation without HUVECs or MSCs, we observed vascularized glomeruli, suggesting that paracrine effects of these cells may also be minimal (Supplemental Figure 5H). The presence of double-layered basement membrane might be caused by the incomplete fusion between those derived from human podocytes and mouse endothelial cells, as observed when mouse embryonic kidney was transplanted onto a quail chorioallantoic membrane.[46] Therefore, the identification of optimal sources for human endothelial cells is necessary.

While it is difficult to estimate the gestational age on the basis of the morphology of the individual glomeruli,[47,48] waiting for a longer period after transplantation may help further maturation of induced podocytes. However, we observed an excessive growth of stromal, presumably nonrenal, cells in the transplants. Thus, it will be essential to develop methods to purify nephron progenitors for transplantation. At the same time, it is necessary to induce genuine stromal cells because both interstitial cells and mesangial cells are derived from renal stromal progenitors.[45] At present, we have no evidence that proper mesangial cells exist in our vascularized glomeruli. Ideally, human endothelial and mesangial cells that correspond to those in the developing kidney should be combined. Although further induction studies, as well as imaging techniques to visualize the slit diaphragm with a higher resolution,[49] are needed to achieve this goal, our results will accelerate the understanding of human podocyte biology both in developmental and diseased states.

CONCISE METHODS

Generation of *NPHS1-TALEN* Plasmids and Validation of Their Activity

NPHS1-TALENs were designed to bind the following sequences to cleave close to the starting codon of *NPHS1*: 5′-TGGCCCTGGGGACGACGC-3′ for the left TALEN and 5′-TCAGCAGCCCCAGGAGCA-3′ for the right TALEN (the underlined sequence corresponds to the latter two thirds of the starting codon). Platinum Gate TALEN Kit (Addgene; Kit #1000000043) was used to construct a TALEN expression vector as described previously.[50] A *CAG* promoter–driven vector was used as the destination vector. To evaluate mutagenic efficiency, *NPHS1*-TALENs were transfected into HEK293 cells using Lipofectamine 2000 (Life Technologies). The target region was amplified using the following primers: 5′-AAAGAAAAGCAGGTGGCAGA-3′ and 5′-AAAGGGCAGAGGGTTTGTCT-3′. When the fragment was denatured and annealed, we observed a clear band shift that indicated formation of a mismatched duplex resulting from deletions or insertions.[51] The amplified fragment was then cloned into pCRII-TOPO (Invitrogen) and 10 clones were sequenced (Supplemental Figure 1A).

Generation of *NPHS1-GFP* iPS Cells

The human iPS cell line (201B7) was maintained on mouse embryonic fibroblasts as described elsewhere.[52] The cells were pretreated with Y27632 (10 μM) 1 hour before electroporation and were dissociated into single cells with collagenase-containing trypsin solution (CTK:

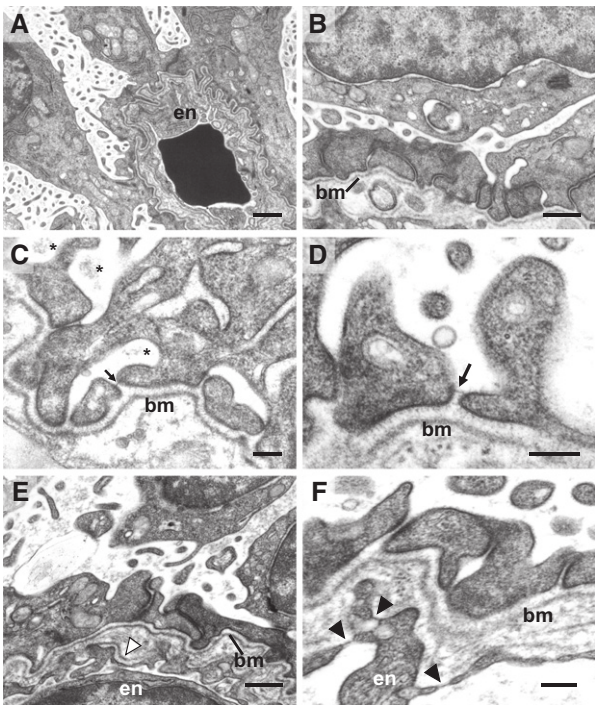

Figure 7. iPS cell–derived glomeruli in the transplants exhibited many morphologic features of those *in vivo*. (A) Induced podocytes surrounding the vascular endothelial cells and extending many cell processes, shown by transmission electron microcopy. (B) Complex cell processes of podocytes formed between the cells and above the basement membrane. (C and D) Formation of slit diaphragm–like structures (arrows) between the cell processes of induced podocytes. Note the electron-dense substance in the Bowman's capsule (asterisk). (E) Formation of double-layered basement membranes, each derived from endothelial cells (white arrowheads) and induced podocytes. (F) Fenestrated endothelial cells with diaphragms (black arrowheads). bm, basement membrane derived from induced podocytes; en, endothelial cells. Scale bars: A: 1 μm; B, E: 0.5 μm; C, D, F: 0.2 μm.

ReproCELL) followed by Accutase (Millipore); 5′ and 3′ homology arms (0.87 kb and 0.92 kb, respectively) of *NPHS1* were then amplified from the genomic DNA of the iPS cells using the following primers: 5′-ggatccGGGAGACCACCTTGATCTGA-3′ and 5′-gctagcCACAGGTCCCCCTACTGTGA-3′ for the 5′ homology arm and 5′-ggcgcgccT GCTGACTGAAGGTGAGTGG-3′ and 5′-gcggccgcGGCCCTTAGAAGGGTACTGG-3′ for the 3′ homology arm. Upon sequence verification, these arms were cloned in the *BamHI-Nhe*I and *Asc*I-*Not*I sites, respectively, of the Oct4-eGFP-PGK-PURO vector (obtained from Addgene),[14] such that the starting codon of *NPHS1* was replaced with that of *GFP*. This targeting vector (5 μg), as well as the pair of TALEN plasmids (5 μg each), was electroporated into the dissociated human iPS cells using Super Electroporator NEPA21 (Neppagene) under the following conditions: two poring pulses (125 V, 2.5 msec) followed by five transfer pulses (20 V, 50 msec). Subsequently the cells were plated onto puromycin-resistant DR4 feeders and puromycin (0.25 μg/ml) was added 2 days after electroporation.[53] Six of 12 puromycin-resistant clones were correctly targeted as determined by PCR and Southern blotting analyses. The primers used for PCR screening of 5′ recombination were 5′-AGCACCAGCTACTTGGGAGA-3′ and 5′-AAGTCGTGCTGCTTCATGTG-3′ (product size: 1347 bp), and those for 3′ recombination were 5′-GCCTGAAGAACGAGAATCCAGC-3′ and 5′–ATCTCCCCACACCTTCTCCT-3′ (product size: 1150 bp). PCR amplifications were performed using GoTaq DNA polymerase (Promega) by denaturation at 95°C for 5 minutes, followed by 35 cycles of 95°C for 30 seconds, 58°C for 60 seconds, and 72°C for 30 seconds, and a final extension at 72°C for 7 minutes. The digoxigenin-labeled probes for Southern blot analysis were amplified using the PCR dig probe synthesis kit (Roche Diagnostics) and the following primers: 5′-CAAGTCATGGGGCTGTTTTT-3′ and 5′-TCACATGCTTGACTCCTTGC-3′ for the 5′ probe and 5′-GGCCCTTTTCCTCTAGAACG-3′ and 5′-AATTGGGTCCCAGATGTTCA-3′ for the 3′ probe. GFP faithfully mimicked *NPHS1* expression in the podocytes, without deletion of the puromycin-resistance cassette.

Kidney Induction from *NPHS1-GFP* iPS Cells

The *NPHS1-GFP* iPS clones were induced to nephron progenitors by a method previously established in our laboratory.[13] Subsequently the induced nephron progenitor aggregates were cultured at the air-fluid interface on a polycarbonate filter (0.8 μm; Whatman) supplied with DMEM containing 10% FCS and with mouse embryonic spinal cord taken from E12.5 embryos.[13] Upon confirmation of the capacity of multiple clones to differentiate into glomeruli, clone #3 was maintained in a feeder-free condition as described earlier[54] and mainly used for the detailed analyses. Fifty of 50 analyzed aggregates from seven independent experiments showed GFP expression. Among these, the fluorescent images of four aggregates were taken daily using a macrozoom laser confocal microscope AZ-C1 (Nikon).

Immunohistochemical Analysis

Samples were fixed in 10% formalin, embedded in paraffin, and cut into 6-μm thick sections. Antigen retrieval in citrate buffer was performed before staining. Alternatively, the samples were fixed in 4% formaldehyde for frozen sections. The following primary antibodies were used: guinea pig anti-nephrin (Progen Biotechnik, catalog no. GP-N2); chick anti-GFP (Abcam, catalog no. ab13970); rabbit anti-GFP (Life Technologies, catalog no. A-11122); rabbit anti-WT1 (C19) (Santa Cruz Biotechnology, catalog no. sc-192); rabbit anti-type IV collagen (Rockland Immunochemicals, catalog no. 600–401–106); mouse anti–E-cadherin (BD Biosciences, catalog no. 610181); rabbit anti-cadherin-6 (kind gift from Gregory Dressler)[55]; goat anti-podocalyxin (R&D Systems, catalog no. AF1658); rabbit anti-CD31 (Abcam, catalog no. Ab28364); rat anti-CD31 (BD Biosciences, catalog no. 557355); anti-human CD31 antibody (Thermo Fisher Scientific, catalog no. MA5-15336); anti-mouse endothelial cell antigen (MECA-32: Novus Biologicals, catalog no. 100-77668); and anti-human nuclear antibody STEM101 (Takara Bio, catalog no. Y40400). Secondary antibodies were conjugated with Alexa 488 or 568 (Life Technologies). Immunofluorescence was visualized with an LSM780 confocal microscope (Carl Zeiss) or a TCS SP8 confocal microscope (Leica). Seven samples at day 9 obtained from seven

independent induction experiments *in vitro* were serially sectioned and showed consistent results.

Electron Microscopy

The tissues were fixed in 2.5% glutaraldehyde containing 1% tannic acid buffered with 0.1 M phosphate buffer (PB, pH 7.4), postfixed with 1% OsO4 in 0.1 M PB for 1 hour at 4°C, dehydrated in a graded ethanol series, and embedded in epoxy resin. Ultrathin sections were stained with 4% uranyl acetate and lead citrate and then examined with a JEM 1230 electron microscope (JEOL, Tokyo, Japan). For scanning electron microscopy, samples were fixed in 2.5% glutaraldehyde buffered with 0.1 M PB for 24 hours at 4°C. Samples were sliced with a razor blade into small pieces (1 mm thickness) and postfixed in 2% OsO4 for 2 hours. Subsequently, samples were dehydrated, substituted with t-butyl alcohol, and dried at −20°C in a vacuum. The samples were made electrically conductive by mounting on aluminum slabs with a carbon paste, followed by coating in an osmium plasma coater (Filgen Inc., Nagoya, Japan) to a thickness of approximately 10 nm, and then observed with a Hitachi S-4800 (Tokyo, Japan).

Flow Cytometry

Induced kidney tissues were dissociated by incubation with 0.25% trypsin/EDTA for 5 minutes. The percentage of cells in the GFP-positive fraction was examined in five independent induction experiments. In two of these experiments, further antibody staining was performed. After blocking in normal mouse serum (Thermo Fisher Scientific), staining was carried out in buffer comprising 1% BSA, 1× Hank balanced saline solution, and 0.035% $NaHCO_3$. The extracellular domain of nephrin was stained with a mouse monoclonal antibody (48E11: a kind gift from K. Tryggvason),[19] followed by anti-mouse IgG1 phycoerythrin (eBioscience, catalog no. 12-4015-82). Podocalyxin was stained with a goat anti-podocalyxin antibody (R&D Systems, catalog no. AF 1658) followed by donkey anti-goat Alexa-633 (Life Technologies, catalog no. A21082). Data were obtained using a FACS SORPAria (BD Biosciences) and analyzed with FlowJo software (TreeStar, Inc.). Sorted podocytes were cultured in RPMI1640 with 10% FCS on coverslips coated with laminin-521 (BioLamina). Culture experiments were performed four times.

Quantitative RT-PCR and Microarray Analysis

RNA was isolated using an RNeasy Plus Micro Kit (Qiagen) and then reverse-transcribed with random primers using the Superscript VILO cDNA synthesis kit (Life Technologies). Quantitative PCR was carried out using the Dice Real Time System Thermal Cycler (Takara Bio) and Thunderbird SYBR qPCR Mix (Toyobo). The primer sequences are listed in Supplemental Table 5. All the samples were normalized against β-actin expression. Three pairs of GFP-positive and -negative fractions were subjected to microarray analyses, which were performed using an Agilent Sure Print G3 human gene expression (8×60K) microarray (Agilent Technologies). The microarray data have been deposited in the National Center for Biotechnology Information Gene Expression Omnibus (GSE66969). Enriched genes in the GFP-positive fraction were selected against the GFP-negative fraction, based on the following criteria: increase call at $P<0.05$ by the Benjamini-Hochberg procedure, fold induction >1.5, and raw expression level >150. Similarly, gene sets of adult human glomeruli were compared with those of tubules and interstitial cells (GSE21785).[11] Adult podocytes from *Mafb-GFP* transgenic mice (GSE17142) were compared with adult kidney cortex (GSE42713).[21,56] Furthermore, genes enriched in GFP-positive podocytes or the gene list common to all three comparisons (Supplemental Table 1, Table 1) were applied for cluster analysis against the array from a variety of human tissues (GSE14938).[20] The data were analyzed using unsupervised hierarchical clustering with Canberra or Chebyshev distance, respectively, and average linkage method using GeneSpringGX13.

Transplantation of iPS Cell–Derived Kidney Tissues

We used the parental iPS cell line (201B7) to avoid the potential impairment of differentiation potentials caused by excessive passages. The iPS cell–derived nephron progenitor aggregates were cultured with E12.5 mouse spinal cords *in vitro* for 1 day to initiate tubulogenesis.[13] The 1:1 mixed spheres of HUVECs and MSCs (both from Ronza) were generated in U-bottom low cell-binding plates (Thermo Fisher Scientific; total, 50,000 cells/sphere). Two spacer rods were made in Hematocrit Tubes (DRUMMOND, 1-000-7500-C/5) with 4% agarose (SIGMA A6013) dissolved in PBS. The rods were soaked with recombinant VEGF (5 ng/ml dissolved; R&D Systems, 293-VE) in DMEM/F12 (Life Technologies, 11320-033) containing 10% bovine serum overnight. The host kidney capsule was incised at approximately 2 mm from the caudal end of the kidneys and the rods were carefully inserted in the lateral side with forceps. Inserted rods were arranged to make a V-shaped free space and briefly cauterized with capsule membrane by electric cautery to prevent them shifting from their initial positions. Finally, two iPS-derived aggregates with mouse embryonic spinal cords and two HUVEC/MSC mixed spheres were inserted from the incised window by a 20-gauge plastic indwelling needle connected by a P-200 Gilson pipette. Immunodeficient NOD/SCID/JAK3null mice[57] were used as the host animal and were anesthetized with chloral hydrate (Wako Chemicals; 400 mg/kg body wt). All animal experiments were performed in accordance with institutional guidelines and approved by the licensing committee of Kumamoto University (A27–018).

ACKNOWLEDGMENTS

We thank K. Tryggvason for providing the anti-nephrin antibody (48E11); S. Okada for providing the immunodeficient mice; R. Matoba and M. Hiratsuka for microarray analysis; and S. Fujimura, S. Tanigawa, and the members of the Liaison Laboratory Research Promotion Center in Kumamoto University for technical assistance.

This study was supported by the Japan Science and Technology Agency (CREST); a KAKENHI grant (26253051) from the Ministry of Education, Culture, Sports, Science, and Technology, Japan; and a grant from Japan Agency for Medical Research and Development.

DISCLOSURES

None.

REFERENCES

1. Quaggin SE, Kreidberg JA: Development of the renal glomerulus: Good neighbors and good fences. *Development* 135: 609–620, 2008
2. Schell C, Wanner N, Huber TB: Glomerular development—shaping the multi-cellular filtration unit. *Semin Cell Dev Biol* 36: 39–49, 2014
3. Kestilä M, Lenkkeri U, Männikkö M, Lamerdin J, McCready P, Putaala H, Ruotsalainen V, Morita T, Nissinen M, Herva R, Kashtan CE, Peltonen L, Holmberg C, Olsen A, Tryggvason K: Positionally cloned gene for a novel glomerular protein—nephrin—is mutated in congenital nephrotic syndrome. *Mol Cell* 1: 575–582, 1998
4. Ruotsalainen V, Ljungberg P, Wartiovaara J, Lenkkeri U, Kestilä M, Jalanko H, Holmberg C, Tryggvason K: Nephrin is specifically located at the slit diaphragm of glomerular podocytes. *Proc Natl Acad Sci U S A* 96: 7962–7967, 1999
5. Patrakka J, Tryggvason K: Nephrin—a unique structural and signaling protein of the kidney filter. *Trends Mol Med* 13: 396–403, 2007
6. Boute N, Gribouval O, Roselli S, Benessy F, Lee H, Fuchshuber A, Dahan K, Gubler MC, Niaudet P, Antignac C: NPHS2, encoding the glomerular protein podocin, is mutated in autosomal recessive steroid-resistant nephrotic syndrome. *Nat Genet* 24: 349–354, 2000
7. Donoviel DB, Freed DD, Vogel H, Potter DG, Hawkins E, Barrish JP, Mathur BN, Turner CA, Geske R, Montgomery CA, Starbuck M, Brandt M, Gupta A, Ramirez-Solis R, Zambrowicz BP, Powell DR: Proteinuria and perinatal lethality in mice lacking NEPH1, a novel protein with homology to NEPHRIN. *Mol Cell Biol* 21: 4829–4836, 2001
8. Kobayashi A, Valerius MT, Mugford JW, Carroll TJ, Self M, Oliver G, McMahon AP: Six2 defines and regulates a multipotent self-renewing nephron progenitor population throughout mammalian kidney development. *Cell Stem Cell* 3: 169–181, 2008
9. Carroll TJ, Park JS, Hayashi S, Majumdar A, McMahon AP: Wnt9b plays a central role in the regulation of mesenchymal to epithelial transitions underlying organogenesis of the mammalian urogenital system. *Dev Cell* 9: 283–292, 2005
10. Guo G, Morrison DJ, Licht JD, Quaggin SE: WT1 activates a glomerular-specific enhancer identified from the human nephrin gene. *J Am Soc Nephrol* 15: 2851–2856, 2004
11. Lindenmeyer MT, Eichinger F, Sen K, Anders H-J, Edenhofer I, Mattinzoli D, Kretzler M, Rastaldi MP, Cohen CD: Systematic analysis of a novel human renal glomerulus-enriched gene expression dataset. *PLoS One* 5: e11545, 2010
12. Naruse K, Fujieda M, Miyazaki E, Hayashi Y: An immunohistochemical study of developing glomeruli in human fetal kidneys. *Kidney Int* 57: 1836–1846, 2000
13. Taguchi A, Kaku Y, Ohmori T, Sharmin S, Ogawa M, Sasaki H, Nishinakamura R: Redefining the in vivo origin of metanephric nephron progenitors enables generation of complex kidney structures from pluripotent stem cells. *Cell Stem Cell* 14: 53–67, 2014
14. Hockemeyer D, Wang H, Kiani S, Lai CS, Gao Q, Cassady JP, Cost GJ, Zhang L, Santiago Y, Miller JC, Zeitler B, Cherone JM, Meng X, Hinkley SJ, Rebar EJ, Gregory PD, Urnov FD, Jaenisch R: Genetic engineering of human pluripotent cells using TALE nucleases. *Nat Biotechnol* 29: 731–734, 2011
15. Ruotsalainen V, Patrakka J, Tissari P, Reponen P, Hess M, Kestilä M, Holmberg C, Salonen R, Heikinheimo M, Wartiovaara J, Tryggvason K, Jalanko H: Role of nephrin in cell junction formation in human nephrogenesis. *Am J Pathol* 157: 1905–1916, 2000
16. Bariety J, Mandet C, Hill GS, Bruneval P: Parietal podocytes in normal human glomeruli. *J Am Soc Nephrol* 17: 2770–2780, 2006
17. Brièare N, Magny P: Scanning electron microscopic observations of human fetal kidney maturing in vivo and in serum-free organ culture. *Anat Rec* 235: 461–474, 1993
18. Hyodo T, Naguro T, Kameie T, Iino A, Miyagawa I: Scanning and transmission electron-microscopic study of the development of the podocyte in the human fetus. *Pediatr Nephrol* 11: 133–139, 1997
19. Ruotsalainen V, Reponen P, Khoshnoodi J, Kilpeläinen P, Tryggvason K: Monoclonal antibodies to human nephrin. *Hybrid Hybridomics* 23: 55–63, 2004
20. She X, Rohl CA, Castle JC, Kulkarni AV, Johnson JM, Chen R: Definition, conservation and epigenetics of housekeeping and tissue-enriched genes. *BMC Genomics* 10: 269, 2009
21. Brunskill EW, Georgas K, Rumballe B, Little MH, Potter SS: Defining the molecular character of the developing and adult kidney podocyte. *PLoS One* 6: e24640, 2011
22. Shih NY, Li J, Karpitskii V, Nguyen A, Dustin ML, Kanagawa O, Miner JH, Shaw AS: Congenital nephrotic syndrome in mice lacking CD2-associated protein. *Science* 286: 312–315, 1999
23. Pierchala BA, Muñoz MR, Tsui CC: Proteomic analysis of the slit diaphragm complex: CLIC5 is a protein critical for podocyte morphology and function. *Kidney Int* 78: 868–882, 2010
24. Asanuma K, Campbell KN, Kim K, Faul C, Mundel P: Nuclear relocation of the nephrin and CD2AP-binding protein dendrin promotes apoptosis of podocytes. *Proc Natl Acad Sci U S A* 104: 10134–10139, 2007
25. Xiao Z, Rodriguez PQ, He L, Betsholtz C, Tryggvason K, Patrakka J: Wtip- and gadd45a-interacting protein dendrin is not crucial for the development or maintenance of the glomerular filtration barrier. *PLoS One* 8: e83133, 2013
26. Has C, Spartà G, Kiritsi D, Weibel L, Moeller A, Vega-Warner V, Waters A, He Y, Anikster Y, Esser P, Straub B, Hausser I, Bockenhauer D, Dekel B, Hildebrandt F, Bruckner-Tuderman L, Laube G: Integrin α3 mutations with kidney, lung, and skin disease. *N Engl J Med* 366: 1508–1514, 2012
27. Shukrun R, Vivante A, Pleniceanu O, Vax E, Anikster Y, Dekel B, Lotan D: A human integrin-α3 mutation confers major renal developmental defects. *PLoS One* 9: e90879, 2014
28. Hinkes B, Wiggins RC, Gbadegesin R, Vlangos CN, Seelow D, Nürnberg G, Garg P, Verma R, Chaib H, Hoskins BE, Ashraf S, Becker C, Hennies HC, Goyal M, Wharram BL, Schachter AD, Mudumana S, Drummond I, Kerjaschki D, Waldherr R, Dietrich A, Ozaltin F, Bakkaloglu A, Cleper R, Basel-Vanagaite L, Pohl M, Griebel M, Tsygin AN, Soylu A, Müller D, Sorli CS, Bunney TD, Katan M, Liu J, Attanasio M, O'toole JF, Hasselbacher K, Mucha B, Otto EA, Airik R, Kispert A, Kelley GG, Smrcka AV, Gudermann T, Holzman LB, Nürnberg P, Hildebrandt F: Positional cloning uncovers mutations in PLCE1 responsible for a nephrotic syndrome variant that may be reversible. *Nat Genet* 38: 1397–1405, 2006
29. The May-Hegglin/Fechtner Syndrome Consortium: Mutations in MYH9 result in the May-Hegglin anomaly, and Fechtner and Sebastian syndromes. *Nat Genet* 26: 103–105, 2000
30. Kelley MJ, Jawien W, Ortel TL, Korczak JF: Mutation of MYH9, encoding non-muscle myosin heavy chain A, in May-Hegglin anomaly. *Nat Genet* 26: 106–108, 2000
31. Sison K, Eremina V, Baelde H, Min W, Hirashima M, Fantus IG, Quaggin SE: Glomerular structure and function require paracrine, not autocrine, VEGF-VEGFR-2 signaling. *J Am Soc Nephrol* 21: 1691–1701, 2010
32. Kazama I, Mahoney Z, Miner JH, Graf D, Economides AN, Kreidberg JA: Podocyte-derived BMP7 is critical for nephron development. *J Am Soc Nephrol* 19: 2181–2191, 2008
33. Neumann-Haefelin E, Kramer-Zucker A, Slanchev K, Hartleben B, Noutsou F, Martin K, Wanner N, Ritter A, Gödel M, Pagel P, Fu X, Müller A, Baumeister R, Walz G, Huber TB: A model organism approach: Defining the role of Neph proteins as regulators of neuron and kidney morphogenesis. *Hum Mol Genet* 19: 2347–2359, 2010

34. Takemoto M, He L, Norlin J, Patrakka J, Xiao Z, Petrova T, Bondjers C, Asp J, Wallgard E, Sun Y, Samuelsson T, Mostad P, Lundin S, Miura N, Sado Y, Alitalo K, Quaggin SE, Tryggvason K, Betsholtz C: Large-scale identification of genes implicated in kidney glomerulus development and function. *EMBO J* 25: 1160–1174, 2006
35. Fan X, Li Q, Pisarek-Horowitz A, Rasouly HM, Wang X, Bonegio RG, Wang H, McLaughlin M, Mangos S, Kalluri R, Holzman LB, Drummond IA, Brown D, Salant DJ, Lu W: Inhibitory effects of Robo2 on nephrin: A crosstalk between positive and negative signals regulating podocyte structure. *Cell Reports* 2: 52–61, 2012
36. Hashimoto T, Karasawa T, Saito A, Miyauchi N, Han GD, Hayasaka K, Shimizu F, Kawachi H: Ephrin-B1 localizes at the slit diaphragm of the glomerular podocyte. *Kidney Int* 72: 954–964, 2007
37. Suh JH, Miner JH: The glomerular basement membrane as a barrier to albumin. *Nat Rev Nephrol* 9: 470–477, 2013
38. Takebe T, Sekine K, Enomura M, Koike H, Kimura M, Ogaeri T, Zhang R-R, Ueno Y, Zheng Y-W, Koike N, Aoyama S, Adachi Y, Taniguchi H: Vascularized and functional human liver from an iPSC-derived organ bud transplant. *Nature* 499: 481–484, 2013
39. Takebe T, Enomura M, Yoshizawa E, Kimura M, Koike H, Ueno Y, Matsuzaki T, Yamazaki T, Toyohara T, Osafune K, Nakauchi H, Yoshikawa HY, Taniguchi H: Vascularized and complex organ buds from diverse tissues via mesenchymal cell-driven condensation. *Cell Stem Cell* 16: 556–565, 2015
40. Ichimura K, Stan RV, Kurihara H, Sakai T: Glomerular endothelial cells form diaphragms during development and pathologic conditions. *J Am Soc Nephrol* 19: 1463–1471, 2008
41. Takasato M, Er PX, Becroft M, Vanslambrouck JM, Stanley EG, Elefanty AG, Little MH: Directing human embryonic stem cell differentiation towards a renal lineage generates a self-organizing kidney. *Nat Cell Biol* 16: 118–126, 2013
42. Lam AQ, Freedman BS, Morizane R, Lerou PH, Valerius MT, Bonventre JV: Rapid and efficient differentiation of human pluripotent stem cells into intermediate mesoderm that forms tubules expressing kidney proximal tubular markers. *J Am Soc Nephrol* 25: 1211–1225, 2014
43. Mae S, Shono A, Shiota F, Yasuno T, Kajiwara M, Gotoda-Nishimura N, Arai S, Sato-Otubo A, Toyoda T, Takahashi K, Nakayama N, Cowan CA, Aoi T, Ogawa S, McMahon AP, Yamanaka S, Osafune K: Monitoring and robust induction of nephrogenic intermediate mesoderm from human pluripotent stem cells. *Nat Commun* 4: 1367, 2013
44. Humphreys BD, Lin S-L, Kobayashi A, Hudson TE, Nowlin BT, Bonventre JV, Valerius MT, McMahon AP, Duffield JS: Fate tracing reveals the pericyte and not epithelial origin of myofibroblasts in kidney fibrosis. *Am J Pathol* 176: 85–97, 2010
45. Kobayashi A, Mugford JW, Krautzberger AM, Naiman N, Liao J, McMahon AP: Identification of a multipotent self-renewing stromal progenitor population during mammalian kidney organogenesis. *Stem Cell Reports* 3: 650–662, 2014
46. Sariola H: Incomplete fusion of the epithelial and endothelial basement membranes in interspecies hybrid glomeruli. *Cell Differ* 14: 189–195, 1984
47. Vernier RL, Birch-Andersen A: Studies of the human fetal kidney. *J Pediatr* 60: 754–768, 1963
48. Lizardo-Daudt HM, Edelweiss MI, Dos Santos FT, Schumacher RCA: Diagnosis of the human fetal age based on the development of the normal kidney. *J Bras Patol Med Lab* 38: 135–139, 2002
49. Rice WL, Van Hoek AN, Păunescu TG, Huynh C, Goetze B, Singh B, Scipioni L, Stern LA, Brown D: High resolution helium ion scanning microscopy of the rat kidney. *PLoS One* 8: e57051, 2013
50. Sakuma T, Ochiai H, Kaneko T, Mashimo T, Tokumasu D, Sakane Y, Suzuki K, Miyamoto T, Sakamoto N, Matsuura S, Yamamoto T: Repeating pattern of non-RVD variations in DNA-binding modules enhances TALEN activity. *Sci Rep* 3: 3379, 2013
51. Nakagawa Y, Yamamoto T, Suzuki K-I, Araki K, Takeda N, Ohmuraya M, Sakuma T: Screening methods to identify TALEN-mediated knockout mice. *Exp Anim* 63: 79–84, 2014
52. Takahashi K, Tanabe K, Ohnuki M, Narita M, Ichisaka T, Tomoda K, Yamanaka S: Induction of pluripotent stem cells from adult human fibroblasts by defined factors. *Cell* 131: 861–872, 2007
53. Tucker KL, Wang Y, Dausman J, Jaenisch R: A transgenic mouse strain expressing four drug-selectable marker genes. *Nucleic Acids Res* 25: 3745–3746, 1997
54. Nakagawa M, Taniguchi Y, Senda S, Takizawa N, Ichisaka T, Asano K, Morizane A, Doi D, Takahashi J, Nishizawa M, Yoshida Y, Toyoda T, Osafune K, Sekiguchi K, Yamanaka S: A novel efficient feeder-free culture system for the derivation of human induced pluripotent stem cells. *Sci Rep* 4: 3594, 2014
55. Cho EA, Patterson LT, Brookhiser WT, Mah S, Kintner C, Dressler GR: Differential expression and function of cadherin-6 during renal epithelium development. *Development* 125: 803–812, 1998
56. Brunskill EW, Sequeira-Lopez MLS, Pentz ES, Lin E, Yu J, Aronow BJ, Potter SS, Gomez RA: Genes that confer the identity of the renin cell. *J Am Soc Nephrol* 22: 2213–2225, 2011
57. Okada S, Harada H, Ito T, Saito T, Suzu S: Early development of human hematopoietic and acquired immune systems in new born NOD/Scid/Jak3null mice intrahepatic engrafted with cord blood-derived CD34 + cells. *Int J Hematol* 88: 476–482, 2008

See related editorial, "The Ever–Expanding Kidney Repair Shop," on pages 1579–1581.

This article contains supplemental material online at http://jasn.asnjournals.org/lookup/suppl/doi:10.1681/ASN.2015010096/-/DCSupplemental.